Chapter 50

Performance modeling and cell design for high concentration methanol fuel cells

C. E. Shaffer and C. Y. Wang

The Pennsylvania State University, University Park, PA, USA.

1 INTRODUCTION

The direct methanol fuel cell (DMFC) has become a leading contender to replace the lithium-ion (Li-ion) battery as the power source of choice for mobile devices[1–7] (see **DMFC system design for portable applications**, Volume 4). Primary reasons for the large amount of attention being given to DMFC technology include the potential for higher energy density than Li-ion battery technology (the theoretical energy density of liquid methanol (CH_3OH) fuel is $4800\,Wh\,l^{-1}$, whereas the theoretical energy density of Li-ion batteries is roughly $1000–1500\,Wh\,l^{-1}$[5]), no need for fuel reforming or cell humidification, and simple cell design.[2–4] However, the overall energy-conversion efficiency of current DMFC designs is low; hence, to become a viable contender with Li-ion battery technology, DMFC technology must first increase its practical energy density in watt hours per liter.[2, 3] A critical component in accomplishing this task is the use of highly concentrated methanol fuel.[6, 7]

The basic reactions for a DMFC are given by

$$CH_3OH + H_2O \rightarrow 6H^+ + 6e^- + CO_2 \quad \text{(anode)} \quad (1a)$$

$$\underline{6H^+ + 6e^- + (3/2)O_2 \rightarrow 3H_2O \quad \text{(cathode)}} \quad (1b)$$

$$CH_3OH + (3/2)O_2 \rightarrow 2H_2O + CO_2 \quad \text{(overall)} \quad (1c)$$

The methanol oxidation reaction (MOR) given by equation (1a) occurs primarily on the anode side of the cell, while the oxygen reduction reaction (ORR) given by equation (1b) occurs on the cathode. In DMFCs, however, some methanol crosses over the membrane to the cathode side of the cell where it reacts. This crossed-over methanol has two detrimental effects: (i) it increases the cathode overpotential due to mixed-potential effect in the cathode catalyst layer (CL)[8, 9] (see **Methanol effects on the O_2 reduction reaction**, Volume 2), thereby reducing the cell voltage, and (ii) it reduces the fuel efficiency (methanol is reacted without producing electrical current). We can conveniently characterize the crossed-over methanol using the methanol crossover ratio (MCO):

$$MCO = \frac{i_x}{i + i_x} \quad (2)$$

As noted later in equation (11), MCO is another way to describe fuel efficiency. At a typical operating current of a DMFC, MCO is typically in the range of 0.1–0.3 (corresponding to a fuel efficiency of 90–70%), and becomes higher at lower current densities.

Methanol is transported across the membrane from anode to cathode primarily by two mechanisms: electro-osmotic drag (EOD) and molecular diffusion. Because methanol transport to the cathode increases with methanol concentration for both of these mechanisms, in most traditional DMFC designs, low concentration methanol fuel is required to operate the cell at reasonable voltage and efficiency. This, of course, lowers the energy density of the system. Currently, there is significant research ongoing in an effort to mitigate the methanol crossover in DMFCs, thereby facilitating the use of high concentration methanol fuel. The two conventional approaches for accomplishing this task

Handbook of Fuel Cells – Fundamentals, Technology and Applications. Edited by Wolf Vielstich, Harumi Yokokawa, Hubert A. Gasteiger. Volume 6: *Advances in Electocatalysis, Materials, Diagnostics and Durability*. ISBN: 978-0-470-72311-1.

are altering the membrane[10, 11] and altering the anode fuel delivery system.[12–18]

The ratio of proton conductivity to methanol permeability has been a widely used figure of merit when developing and evaluating different membranes for DMFCs. Unfortunately, membranes with reduced methanol permeability also have lower proton conductivity, and it has been exceedingly difficult to maximize this figure of merit (see **Conductivity, permeability, and ohmic shorting of ionomeric membranes**, Volume 5). Neburchilov *et al.*[10] give a comprehensive review of membranes designed for DMFCs, and categorize the membranes into four groups: Nafion® membranes, non-Nafion® fluorinated membranes (e.g., Dow XUS®, Asahi Glass Flemion®, and membranes from Gore & Associates), composite fluorinated membranes (e.g., zirconium-based and silica-based membranes), and nonfluorinated membranes (e.g., polybenzimidazole (PBI)-based membranes, and PolyFuel polycarbon membranes). Out of the extensive types of membranes reviewed, hydrocarbon (nonfluorinated) membranes (see **Hydrocarbon membranes**, Volume 3) and composite fluorinated membranes (see **Composite perfluorinate membranes**, Volume 3) are expected to have the highest ratio of proton conductivity to methanol permeability, while simultaneously attaining low cost. An alternative approach to membrane methanol crossover mitigation is the design of pore-filled electrolyte membranes, as described by Yamaguchi *et al.*[11] In this approach, the pores of a porous substrate are filled with a polymer electrolyte; the substrate matrix is impermeable to water and methanol, and therefore resists swelling. The polymer electrolyte in the pores can take in water, giving it sufficient proton conductivity, while the lack of electrolyte swelling due to the presence of the matrix reduces the methanol crossover. A largely overlooked factor in the DMFC membrane development is the requirement for facilitated water transport through the membrane. Further discussion of membrane materials is outside the scope of this chapter, but, generally speaking, nearly two-decade membrane development has been futile in terms of raising the methanol concentration in DMFCs.

There have been a variety of methods developed for altering the anode fuel delivery system to reduce MCO.[12–18] These methods include proper design of the anode microporous layer (MPL),[12] using a water barrier to maintain an inundated anode CL,[18] and incorporating a dual-pump system for methanol and water balance along with a membrane electrode assembly (MEA) with low or negative water crossover, as described by Wang *et al.*,[13] and using a porous plate between fuel solution and MEA, as explained by Abdelkareem and Nakagawa.[14] In a somewhat different approach, Kim *et al.*[15] have developed fuel cartridges that use hydrogels; while the details are different, the basic concept of controlling the transport rate of methanol into the anode remains the same. Several other approaches of altering the anode fuel delivery system have also been developed, including those utilizing a graphite-based anode plate and a self-regulated passive fuel feed system, as described by Zhang and Hsing,[16] and Chan *et al.*,[17] respectively.

Solely focusing on methanol transport and crossover in an effort to use highly concentrated methanol fuel only paints part of the picture. Note that water reacts stoichiometrically 1:1 with methanol in the MOR (equation 1a) and is produced in the ORR (equation 1b). A point that is often overlooked is that a great deal of water is lost to the cathode side of the cell through the membrane using typical DMFC MEA designs. With the notable exception of three patents,[13, 18, 19] techniques altering the anode fuel delivery system generally violate water balance in the anode, and thus cannot work in steady state. A fundamental key is to address water balance in the anode by considering water crossover through the membrane from anode to cathode.

Defining the net water transport coefficient, α, as the net water flux across the membrane normalized by the protonic flux, we can characterize the water crossover of different MEAs:

$$\alpha = \frac{N_{\text{mem}}^{\text{H}_2\text{O}}}{i/F} \tag{3}$$

Blum *et al.*[20] proposed a water-neutral state for a DMFC where there is a back flux of one H_2O molecule for every six protons that transport across the membrane from anode to cathode, i.e., $\alpha = -1/6$. The idea, of course, is that, with this water-neutral state, no excess water must be supplied to the anode side of the cell for reaction; all of the water necessary for the MOR comes from the production of the ORR on the cathode side, i.e., pure methanol fuel can theoretically be used. MEAs designed to reduce or reverse the net transport of water into the cathode are commonly referred to as *low-α MEA technology*,[7] for which much of the pioneering work was performed by Wang and coworkers;[6, 7, 21–24] Table 1 lists a few milestones and important experimental confirmations for low-α MEA development.

Lu *et al.*,[6] Liu *et al.*,[7] and Wang and Liu[22] illustrated quantitatively how, in order to use highly concentrated methanol fuel, the water crossover to the cathode must first be reduced. For example, Liu *et al.*[7] showed that, in order to use even 3 M methanol fuel, we must have a maximum of $\alpha \approx 3$; a higher value indicates that the cell will run short of water before methanol. Considering that 3 M methanol fuel is only roughly 10% methanol by volume, and that DMFCs not using low-α MEAs generally have $\alpha \approx 3$, this finding is rather astonishing. Lu *et al.*,[6] Liu *et al.*,[7] Wang and Liu,[22] and Liu[23, 24] further demonstrated that, by using a thin Nafion 112 membrane along with hydrophobic anode and cathode MPLs, they could reduce water crossover to $\alpha \sim 0.3$–0.8 at 60 °C while still maintaining a high fuel efficiency (∼80%), cell

Table 1. Milestones and important experimental confirmations in low-α MEA technology.

Reference	α	aMPL/cMPL	Membrane	i (mA cm^{-2})	T (°C)	c_l^{MeOH}(M)	Stoichiometry a/c @ i_{ref}(mA cm^{-2})	Notes/Significance for Given Reference
C. Lim and C. Y. Wang [21]	*n/a*	aMPL and cMPL; both 40 wt% PTFE	Nafion® 112		60, 90	2		First published design of low-α MEA; 210 and 105 mW cm^{-2} max power @ 90 °C and 60 °C.
A. Blum *et al.* [20]	~0.5–0.7	No aMPL; similar to cMPL with PTFE	NP-PCM[a]			1–6		Low performance (<12.5 mW cm^{-2}); proposed water-neutral state.
G. Q. Lu *et al.* [6]	~0.6	aMPL and cMPL; both 40 wt% PTFE	Nafion® 112	~150	60	2	2/4 @ 150	Maximum power density of ~55–60 mW cm^{-2}.
F. Liu *et al.* [7]	~0.8	aMPL and cMPL; both 40 wt% PTFE	Nafion® 112	~150	60	3	2/3 @ 150	First to quantatively show effect of thin membrane in low-α MEA; ~50–60mW cm^{-2} maximum power; first to fully elucidate H_2O management importance for HC-MFC.
	~1.0	aMPL and cMPL; both 40 wt% PTFE	Nafion® 1135	~150	60	3	2/3 @ 150	
C. Y. Wang and F. Liu [22]	~0.6	aMPL and cMPL; both 40 wt% PTFE	Nafion® 112	~150	60	10	1.2/3 @ 150	Low α with high concentration methanol fuel.
	~0.0	aMPL and cMPL; both 40 wt% PTFE	Nafion® 112	~150	60	20	1.3/3 @ 150	
F. Q. Liu [23, 24]	~1.2	cMPL only; 40 wt% PTFE	Nafion® 112	~150	60	2	2/3 @ 150	First to experimentally show hydrophobic aMPL effect on α.
	~0.3	aMPL and cMPL; both 40 wt% PTFE	Nafion® 112	~150	60	2	2/3 @ 150	

(*continued overleaf*)

Table 1. (*continued*).

Reference	α	aMPL/cMPL	Membrane	i (mA cm^{-2})	T (°C)	c_l^{MeOH}(M)	Stoichiometry a/c @ i_{ref}(mA cm^{-2})	Notes/Significance for Given Reference
K.Y. Song *et al.* [25]	∼1.0–2.5	aMPL and cMPL; both 23 wt% PTFE	Nafion® 1135	∼120	60	3	2/air breathing	1.0–2.5 variance due to different cathode BL properties; confirms cMPL effect on α; further confirms membrane thickness effect on α.
	∼2.7	aMPL only; 23 wt% PTFE	Nafion® 1135	∼120	60	3	2/air breathing	
	∼2.7	aMPL and cMPL; both 23 wt% PTFE	Nafion® 115	∼120	60	3	2/air breathing	
J.Y. Park *et al.* [26]	∼3.5	cMPL only; 23 wt% PTFE	Nafion® 1135	∼160	70			Confirms aMPL effect on α; maximum power density of ∼ 90 mW cm^{-2}, but α∼2–4x greater than reported by Lu *et al.*, Liu *et al.*, and Liu with Nafion 112 and two MPLs.
	∼1.1	aMPL and cMPL; both 23 wt% PTFE	Nafion® 1135	∼160	70			

[a] NP-PCM: Nano-Porous Proton Conducting Membrane

voltage (∼0.4 V), and power density (∼60 mW cm^{-2}). The hydrophobic cathode MPL/thin membrane combination in the low-α MEA was believed to be the primary reason for low water crossover, owing to a buildup of liquid pressure in the cathode CL, and corresponding back diffusion and backflow of water due to hydraulic permeation (HP).[2, 19, 27]

Liu *et al.*[7] and later Song *et al.*[25] experimentally found that a thin membrane reduces α. Liu *et al.*[7] showed that α jumped from ∼0.8 to ∼1.0 simply by removing a Nafion® 112 membrane and replacing it with a Nafion® 1135 membrane, and Song *et al.*[25] reported α values of ∼1.0 and ∼2.7 for Nafion® 1135 and Nafion® 115, respectively (see Table 1 for more details). Subsequently, several researchers have also experimentally confirmed that a hydrophobic cathode MPL acts to reduce α. For example, Song *et al.*[25] have reported α values of ∼2.7 and ∼1.0 −2.5 for an MEA without and with hydrophobic cathode MPL, respectively (see Table 1 for more details).

More recently, it was surprisingly discovered that the incorporation of a hydrophobic anode MPL can greatly reduce the water crossover from anode to cathode, playing an even more significant role than the hydrophobic cathode MPL.[23, 24] Utilizing a Nafion® 112 membrane, Liu[23, 24] first demonstrated experimentally that α dropped from ∼1.2 to ∼0.3 in his MEA by simply incorporating a hydrophobic anode MPL. Later, Park *et al.*[26] confirmed the dramatic effect of the hydrophobic anode MPL, reporting α values of ∼3.5 and 1.1 without and with hydrophobic anode MPL, respectively. The nearly fourfold larger α value reported by Park *et al.*[26] for MEAs with hydrophobic anode MPL (1.1 vs. 0.3) may be due to the fact that they used a thicker Nafion® 1135 membrane. Xu *et al.*[28] further give credence to the concept of a hydrophobic anode MPL reducing α, as the authors achieved no lower than α ∼ 2.4 with a Nafion® 112 based MEA with only hydrophobic cathode MPL. Most recently, Shaffer and Wang[29] have physically described how the hydrophobic anode MPL acts to reduce water crossover to the cathode by utilizing a two-phase transport model that fully accounts for capillary-induced flow in porous media.

2 WATER TRANSPORT

Following the mass balance analysis of Liu *et al.*,[7] Figure 1 gives the maximum allowable methanol fuel concentration as a function of α, assuming $MCO = 0.0$, 0.1, 0.2, 0.3, and 0.4. If an actual fuel concentration is greater than that given in Figure 1, the cell runs short on water before it runs short on methanol. This figure clearly illustrates the point that, if we want to use high concentration methanol fuel, we must first limit α to a very low level; this further shows how clearly low-α MEA technology is a critical prerequisite for designing high concentration

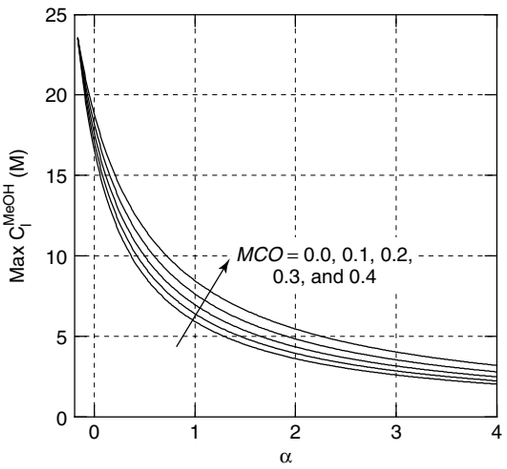

Figure 1. Maximum methanol concentration to maintain methanol and water balance in the anode as a function of α for $MCO = 0.0$, 0.1, 0.2, 0.3, and 0.4.

methanol fuel cells (HC-MFCs). For example, assuming that $MCO = 0$, if we desire to use 10 M methanol fuel, we must be able to design an MEA that has α as low as 0.39. Further note from Figure 1 that, because the slope of the curve is steeper as α becomes lower, as we reduce α we get a greater return on being able to increase the maximum methanol concentration, i.e., the same reduction in α becomes more effective at low α values. This simple example underscores the absolute importance of reducing the water crossover from anode to cathode for successful use of high concentration methanol fuel.

Pasaogullari and Wang[27, 30] outline the theory of liquid flow in fuel cell diffusion media caused by capillary action (see **Two-phase flow and transport**, Volume 3). The total liquid flux through a porous medium is given by Darcy's law

$$\vec{N}_l = -\frac{\rho_l K k_{rl}}{M_l \mu_l} \nabla p_l \tag{4}$$

Here, the capillary pressure is defined as the gas-phase pressure less the liquid-phase pressure, and, assuming that the gas-phase pressure changes negligibly over the thickness of the porous media, the gradient in capillary pressure is equal to the negative of the gradient in liquid pressure, yielding

$$\vec{N}_l = \frac{\rho_l K k_{rl}}{M_l \mu_l} \nabla p_c \tag{5}$$

The capillary pressure can be related to the liquid saturation (i.e., the liquid volume fraction of the pore space) via the Leverett function:

$$p_c = \sigma \cos(\theta) \left(\frac{\varepsilon}{K}\right)^{1/2} J(s) \tag{6}$$

This results in the following expression:

$$\vec{N}_1 = \frac{\rho_1 K k_{rl}}{M_1 \mu_1} (K\varepsilon)^{1/2} (\sigma \cos\theta) \frac{dJ}{ds} \nabla s \tag{7}$$

The details may be found in Pasaogullari and Wang,[27] but the end result is that, within a given porous layer, there is always liquid flow from high liquid saturation region to low liquid saturation region. In addition, note that, across an interface between two inhomogeneous porous layers, the capillary pressure must remain continuous, thereby yielding a saturation jump.[30] This physics is critical in describing how MPLs are effective in reducing α, as discussed later.

On the anode side of the cell, the capillary action acts to transport the methanol–water mixture from the flow channel to the CL. The flux of a given species, β, in the liquid phase can be represented by a convective flux (here X_1^β is the liquid-phase mole fraction of species β) plus a diffusion flux:

$$\vec{N}_l^{\,\beta} = X_l^\beta \vec{N}_l + \vec{j}_l^{\,\beta} \tag{8}$$

The liquid phase is a binary mixture of methanol and water (negligible dissolved CO_2 concentration), and therefore the concentration gradients must be in opposite directions of one another.

Utilizing the 1D (through-plane), two-phase model, as described in Ref. [29] (which fully accounts for the liquid flow driven by capillary action as described by equation (8)), Figure 2 illustrates the liquid methanol and H_2O profiles across the anode diffusion media for $MCO = 0$ (the ideal situation) and $\alpha = 3.0$, 2.0, and 1.0. Unless otherwise noted, the properties of all cells simulated in this article are given in Table 2. It is important to note in these plots that a perfectly horizontal line signifies an equivalent molar ratio of methanol to H_2O at the backing layer (BL), flow channel interface, and in the anode CL. These horizontal lines indicate the following equivalent ratio (under steady state conditions):

$$\left.\frac{\begin{pmatrix}\text{CH}_3\text{OH reacted} + \\ \text{CH}_3\text{OH crossed over}\end{pmatrix}}{\begin{pmatrix}\text{H}_2\text{O reacted} + \\ \text{H}_2\text{O crossed over}\end{pmatrix}}\right|_{\text{molar}} = \left.\frac{(\text{CH}_3\text{OH})}{(\text{H}_2\text{O})}\right|_{\substack{\text{molar} \\ \text{fuel feed}}} \tag{9}$$

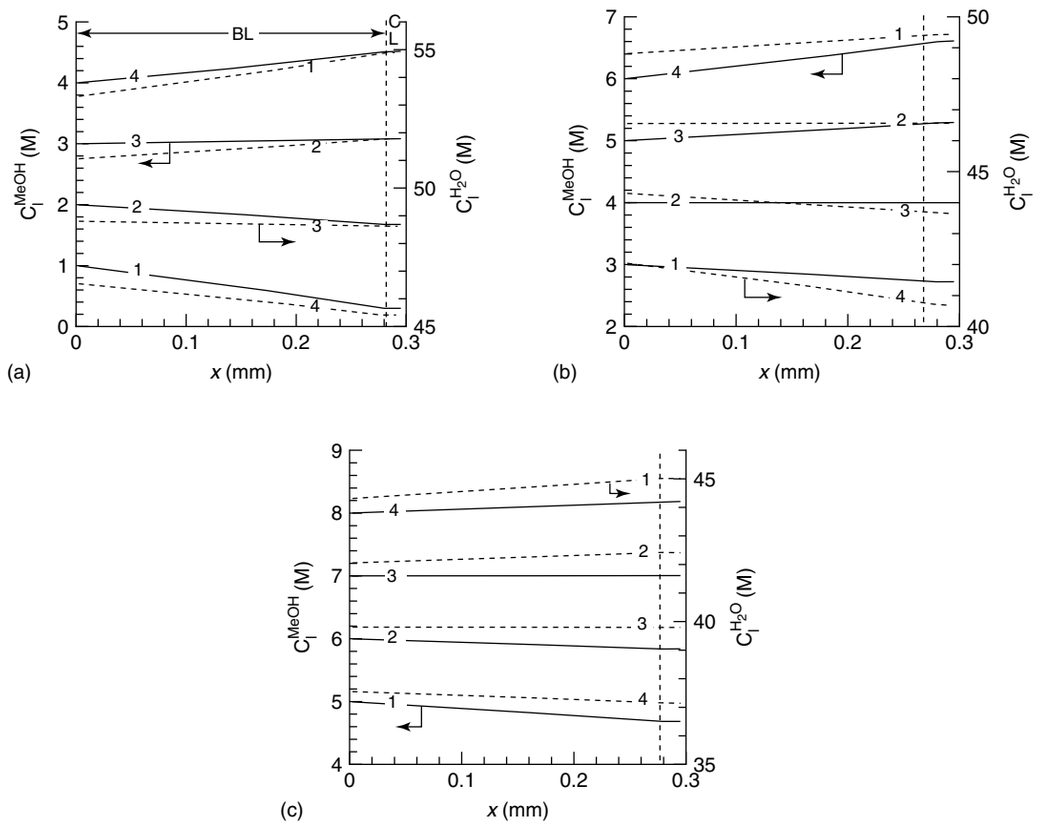

Figure 2. Liquid CH_3OH and H_2O concentration profiles for $MCO = 0$, $i = 150\,\text{mA cm}^{-2}$, and (a) $\alpha = 3.0$, (b) $\alpha = 2.0$, and (c) $\alpha = 1.0$. Curves 1, 2, 3, and 4 stand for the corresponding profiles for the various boundary methanol concentrations at $x = 0$. Note $x = 0$ is at the anode BL and channel interface; $x = 0.295\,\text{mm}$ is at the anode CL and membrane interface.

Table 2. Cell properties and simulation parameters used in this study unless otherwise noted.

Parameter	Value	Notes
$\delta_{BL}(\mu m)$[a]	260 w/ MPL 280 w/o MPL	Anode and cathode
$\delta_{MPL}(\mu m)$	20	Anode and cathode, if present
$\delta_{CL}(\mu m)$	15	Anode and cathode
$\delta_{mem}(\mu m)$	50	Nafion® 112
ε_{BL}, ε_{CL}	0.6	Anode and cathode
ε_{MPL}	0.4	Anode and cathode
K_{BL} (m^2)	1.0×10^{-14}	Anode and cathode
K_{MPL} (m^2)	2.0×10^{-15}	Anode and cathode
K_{CL} (m^2)	3.6×10^{-16}	Anode and cathode
K_{mem} (m^2)	4.0×10^{-20}	
θ_{BL} (°)	110	Anode and cathode
θ_{MPL} (°)	120	Anode and cathode
θ_{CL} (°)	96	Anode and cathode
Temperature (°C)	60	

[a] Note that the different BL thicknesses with and without MPL are to ensure equivalent thickness of the diffusion media and to study the effects of the MPL properties on the water and methanol crossover

Therefore, from Figure 2 we see that, as α decreases, the methanol concentration, to maintain this equivalency, increases: roughly 2–3 M, 4 M, and 7 M for $\alpha = 3.0$, 2.0, and 1.0 respectively. These plots are very useful in demonstrating that, even for an ideal membrane that blocks all methanol transport from the anode to cathode, developing an MEA with low (even negative) water crossover is critically important in designing a DMFC with high energy density operating on highly concentrated methanol fuel.

It is important to note in Figure 2 that an increasing methanol concentration toward the anode CL (positive x direction) only implies a *diffusion* flux in the binary liquid phase away from anode CL (negative x direction). This does not imply a net transport of methanol away from the anode CL, a fact which is illustrated by looking at equation (8). Here, we see that the capillary-induced liquid flow can facilitate a net flux of methanol toward the anode CL (positive x direction), against a concentration gradient, when methanol concentration becomes high. This is exactly what we see in Figure 2, and exactly the same concept that holds for H_2O transport through the porous media.

Any realistic membrane, however, has some degree of methanol crossover. The methanol flux across the membrane is driven by EOD and diffusion, and can be written as

$$N_{mem}^{CH_3OH} = n_d^{CH_3OH}\left(\frac{i}{F}\right) + D_{mem}^{CH_3OH}\left(\frac{c_{l,aCL}^{CH_3OH} - c_{l,cCL}^{CH_3OH}}{\delta_{mem}}\right) \tag{10}$$

Here, the first term is the EOD flux term and the second term signifies the diffusion flux term. The methanol diffusion flux across the membrane is obviously a function of the methanol concentration in the anode CL, and so too is the EOD flux due to the EOD coefficient dependence on methanol concentration. Therefore, for reasons of reducing the MCO, it is important to reduce the methanol concentration in the anode CL. As shown in Figure 3 (as well as Figure 2), one effective way of accomplishing this is by reducing α for a given methanol concentration. Physically, the less water lost to the cathode side of the cell, the lower the methanol concentration in the anode CL. Note that, in Figure 3, we set $MCO = 0.1$ to highlight this point; in reality, the MCO is dynamically a function of the methanol concentration.

As an additional example of the importance of water management on using high concentration methanol fuel, we give a hypothetical cell design with the MCO determined dynamically, and membrane water crossover set to zero ($\alpha = 0.0$). Figure 4 illustrates the liquid methanol concentration profile in the anode under 10 M feed concentration. This cell has an additional porous barrier between BL and CL with $\varepsilon = 0.25$, $\theta = 120°$, and $\delta = 250\,\mu m$ and all other properties are the same as given in Table 2 for a BL. The MCO is simulated to be $MCO = 0.13$ at $i = 250\,mA\,cm^{-2}$, which is due in large part to the reduction of methanol concentration in the anode CL, as seen in Figure 4. The point to take here is that, if we can design an MEA that reduces $\alpha \sim 0$ while simultaneously adding a barrier to methanol and water transport in the anode, we can operate the cell at a high fuel efficiency ($MCO = 0.13$) while using high concentration fuel (10 M), all without external means of water recovery. Here, the barrier between the anode BL and CL provides not only a high resistance to methanol transport but also prevents water from diffusing back from the anode CL into the flow channel.

As a final example of the importance of water crossover on high concentration DMFC performance, Figure 5 shows fuel efficiency curves for $\alpha = 0.0$, 1.0, and 2.0 for (a) 5 M and (b) 3 M methanol fuel concentrations. Note that the fuel efficiency is defined as

$$\eta_f = \frac{i}{i + i_x} = 1 - MCO \tag{11}$$

It is evident from Figure 5 that the fuel efficiency increases with lower α as should be expected from the previous discussions on reducing MCO via lower methanol concentration in the anode CL. It should now be unambiguous how water management plays a critical role for the use of highly concentrated methanol fuel in DMFCs.

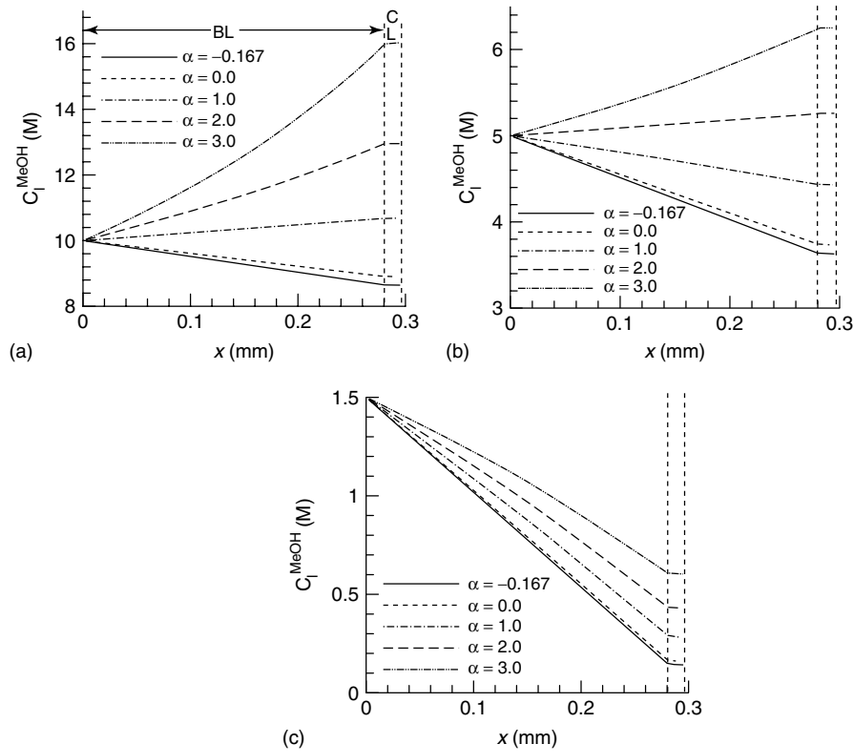

Figure 3. Liquid methanol concentration profiles for $MCO = 0.1$, $i = 200\,\text{mA cm}^{-2}$, and $\alpha = 3.0$, 2.0, 1.0, 0.0, and $-1/6$ for (a) 10 M, (b) 5 M, and (c) 1.5 M boundary methanol concentrations. Note $x = 0$ is at the anode BL and channel interface; $x = 0.295$ mm is at the anode CL and membrane interface.

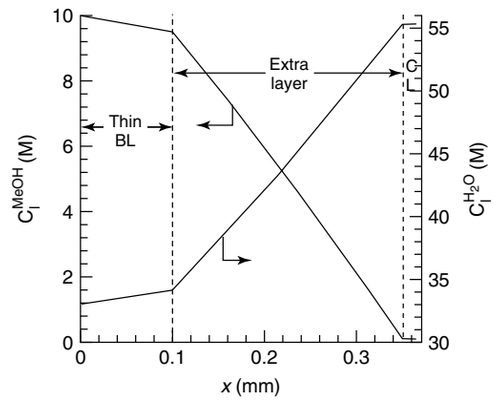

Figure 4. Liquid CH_3OH and H_2O anode concentration profiles for $\alpha = 0.0$, and $i = 250\,\text{mA cm}^{-2}$. The extra layer between BL and CL has all BL properties given in Table 2 except $\varepsilon = 0.25$, $\theta = 120^\circ$, and $\delta = 250\,\mu\text{m}$. Note that $x = 0$ is at the anode BL and channel interface.

3 NOVEL MEA DESIGNS FOR LOW CROSSOVER OF METHANOL AND WATER

Now that it is clear how and why water management plays such a vital role in using highly concentrated methanol fuel, we next review novel MEA designs for low crossover of water. The traditional MEA for DMFCs has a BL and CL on each side of the membrane. The BLs are usually made of either carbon paper or carbon cloth. With the advent of lowα MEA technology, it has become common to use a hydrophobic MPL between the cathode BL and CL in an effort to reduce the water crossover.[6, 7, 19–21, 25, 27, 28] Most recently Liu[23, 24] and Park *et al.*[26] have further demonstrated experimentally the need of a hydrophobic anode MPL to significantly lower α.

Figure 6 shows α values and their EOD, diffusion, and HP components versus current density, as defined by

$$\alpha = n_d^{H_2O} + D_{mem}^{H_2O}\left(\frac{\rho_{mem}}{EW_{mem}}\right)\left(\frac{\lambda_a - \lambda_c}{\delta_{mem}}\right)\left(\frac{F}{i}\right) + \left(\frac{\rho_l K_{mem}}{M_l \mu_l}\right)\left(\frac{p_{l,a} - p_{l,c}}{\delta_{mem}}\right)\left(\frac{F}{i}\right) \quad (12)$$

$$\alpha_{EOD} = n_d^{H_2O} \quad (13a)$$

$$\alpha_{diff} = D_{mem}^{H_2O}\left(\frac{\rho_{mem}}{EW_{mem}}\right)\left(\frac{\lambda_a - \lambda_c}{\delta_{mem}}\right)\left(\frac{F}{i}\right) \quad (13b)$$

$$\alpha_{HP} = \left(\frac{\rho_l K_{mem}}{M_l \mu_l}\right)\left(\frac{p_{l,a} - p_{l,c}}{\delta_{mem}}\right)\left(\frac{F}{i}\right) \quad (13c)$$

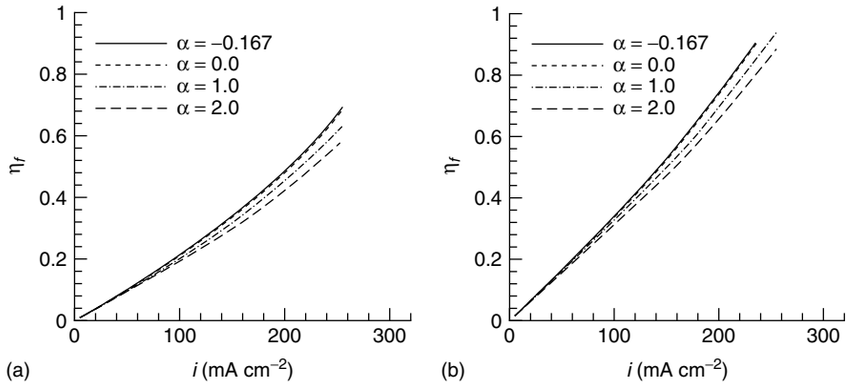

Figure 5. Fuel efficiency versus current density for (a) 5 M and (b) 3 M methanol fuel concentrations; note anode and cathode stoichiometries of 1.75 @ at 150 mA cm^{-2}.

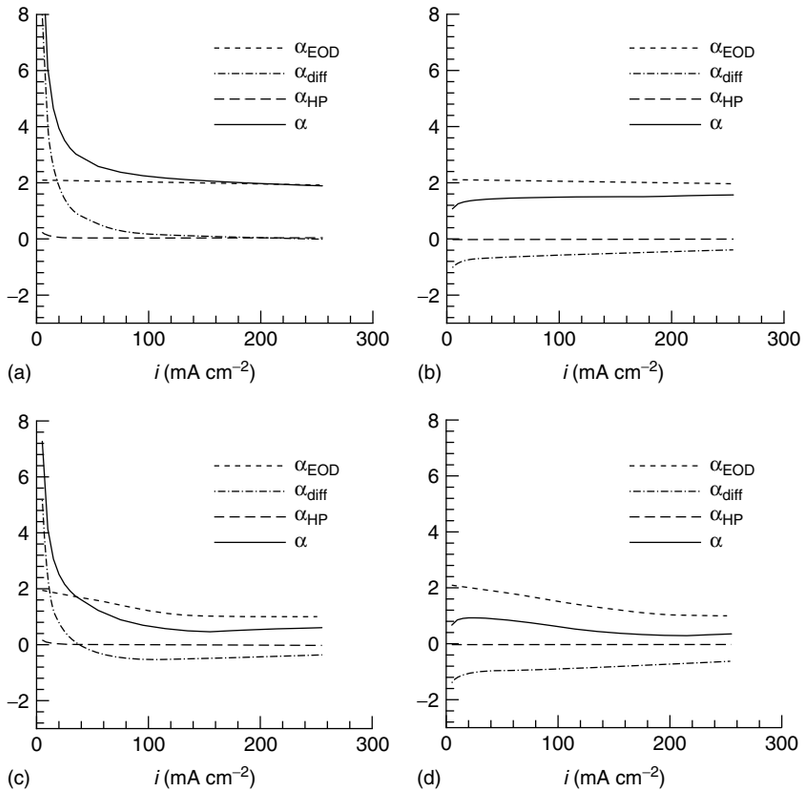

Figure 6. Net water transport coefficient and its EOD, diffusion, and hydraulic permeation components for (a) no MPLs, (b) cathode MPL, (c) anode MPL, and (d) anode and cathode MPLs. Note all hydrophobic MPLs with assumed properties given in Table 2; anode and cathode stoichiometries of 1.75 @ 150 mA cm^{-2} with 3 M fuel.

These simulation results are shown with four different hydrophobic MPL combinations: (a) no MPLs, (b) cathode MPL only, (c) anode MPL only, and (d) anode and cathode MPLs. Table 3 also shows the simulated α and MCO values for the four different MPL combinations at 200 mA cm^{-2}. It is seen that the incorporation of a hydrophobic cathode MPL slightly reduces α (1.97 without MPLs to 1.52 with cathode MPL at 200 mA cm^{-2}), but the use of a hydrophobic anode MPL reduces α more drastically (1.97 without MPLs to 0.544 with anode MPL at 200 mA cm^{-2}). The use of both anode and cathode hydrophobic MPLs lowers α the most (1.97 without MPLs to 0.293 with both MPLs at 200 mA cm^{-2}). Further, note that the incorporation of hydrophobic anode and cathode MPLs also slightly reduces the MCO (on the order of 10%). These simulated results for MPL effects

on both α and MCO are in qualitative agreement with experimental observations and the theory presented by several researchers.[6, 7, 23–27]

The theory of how hydrophobic anode and cathode MPLs act together to reduce water crossover is elucidated for the first time by Shaffer and Wang.[29] The liquid saturation profiles given in Figure 7 help in explaining physically how the MPLs cause this significant reduction in α. In Figure 7 (a), we see that the cathode MPL acts to increase the liquid saturation level in the cathode CL, thereby increasing both the back diffusion and potentially backflow of H_2O due to HP (see equations 12 and 13). This fact is also depicted by comparing Figure 6(a) and (b), where it is evident that the incorporation of the cathode MPL significantly reduces the diffusion component of water crossover. Physically, the hydrophobic cathode MPL leads to a higher liquid pressure at the cathode MPL/CL interface, and, because the liquid pressure is uniform across the interface (see, e.g., Ref. [30]), a corresponding higher liquid saturation level is reached in the cathode CL.

Table 3. α and MCO values for four MPL combinations at 200 mA cm^{-2}. Note all parameters given in Table 2; anode and cathode stoichiometries of 1.75 @ 150 mA cm^{-2} with 3 M fuel.

MPL Combination	α	MCO
No MPLs	1.97	0.345
Cathode MPL	1.52	0.327
Anode MPL	0.544	0.305
Two MPLs	0.293	0.294

The effects of a hydrophobic anode MPL are evident from Figure 7(b). We see here that a hydrophobic anode MPL greatly reduces the liquid saturation level in the anode MPL, and ultimately reduces the liquid saturation level in the anode CL; in fact, under these conditions, the anode CL is predicted to become gas-phase only. This CL condition leads to a lower water crossover from anode to cathode, primarily by reducing the EOD (note that the EOD coefficient is a function of membrane water content), and by an increase in back diffusion, as depicted further in Figure 6(c) and equations 12 and 13. The lower anode CL saturation in the presence of anode MPL can be explained once again by the lower liquid saturation level in the anode MPL, owing to its hydrophobic nature.

Finally, Figure 7(c) shows the liquid saturation profile for both hydrophobic anode and cathode MPLs. The reduction in α with the two MPL design is explained simply by the

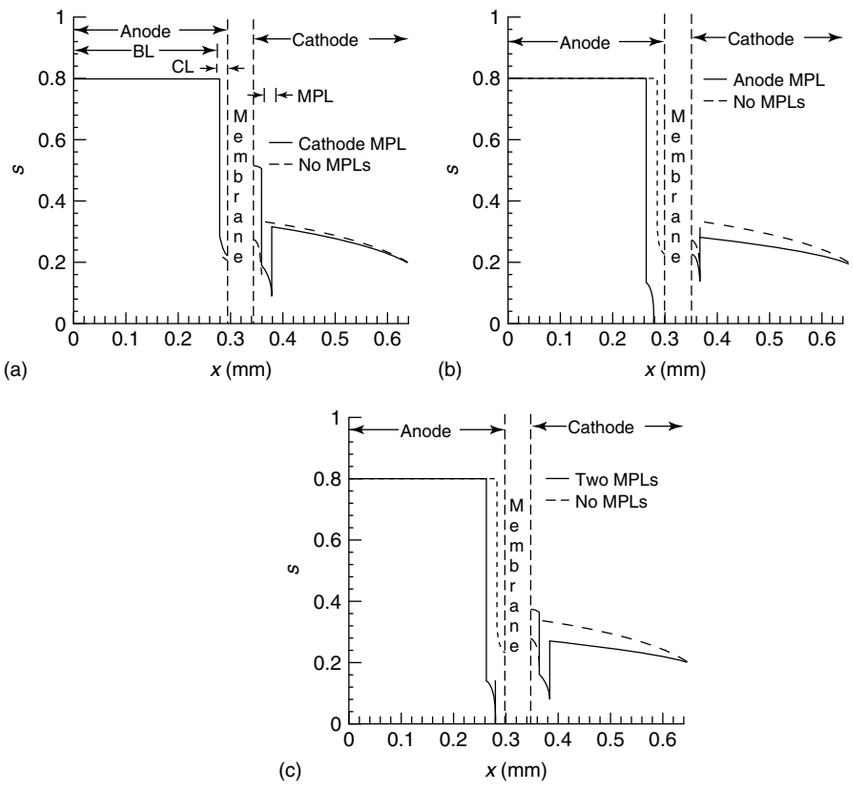

Figure 7. Liquid saturation profiles at $i = 200$ mA cm^{-2} for (a) cathode MPL, (b) anode MPL, and (c) anode and cathode MPLs. Note all hydrophobic MPLs with assumed properties given in Table 2; anode and cathode stoichiometries of 1.75 @ 150 mA cm^{-2} with 3 M fuel; $x = 0$ is at the anode BL and channel interface.

combination of anode and cathode MPL discussions. We should mention that the presence of back diffusion of H_2O from cathode to anode – which is most significant with both anode and cathode MPLs present – is precisely the reason that a thin membrane is generally necessitated in low-α MEAs; the thinner the membrane, the greater the flux of H_2O back diffusion, as evident in equation 13(b).

4 ADVANCED DESIGNS

As alluded to earlier, and further illustrated in Table 1, one of the most important developments in reducing the water crossover in DMFCs is the incorporation of a hydrophobic anode MPL.[23, 24, 26, 29] Here, we briefly summarize the effects of anode MPL properties on water crossover, as described in more detail in Ref. [29]. Figures 8–10 give the simulated α versus current density curves for various values of anode MPL contact angle, permeability, and thickness; note that the operating conditions of 2.0 anode and cathode stoichiometries (at 150 mA cm^{-2}), and inlet methanol concentration of 2.0 M are different from the 1.75 and 3.0 M values for Figures 6 and 7. Further note that, for the simulations given in Figures 8–10, a hydrophobic cathode MPL is present.[29] From these results, we find that a larger contact angle (more hydrophobic), smaller permeability, and thicker anode MPL all act to reduce the water crossover. For all except the thickness effect, the primary reason for lowering α stems from the effect of these properties on the saturation jump at the anode BL/MPL interface; all properties that reduce α reduce the saturation level in the anode MPL. The thicker anode MPL acts to mitigate water crossover simply by forcing the liquid to transport a longer distance, resulting in a lower liquid saturation level at the anode CL–anode MPL interface.

Finally, Tables 4 and 5 give the simulated membrane thickness and H_2O membrane diffusivity effects on net water transport coefficient for an MEA design with hydrophobic anode and cathode MPLs. It is seen that a thinner membrane and membrane with greater H_2O diffusivity actually reduce water loss to the cathode. Table 4 shows that $\alpha = 0.293$ for a membrane thickness of 50 μm (roughly Nafion® 112) and $\alpha = 0.695$ for a thickness of 175 μm (roughly Nafion® 117) from simulated results; Table 5 illustrates that a membrane H_2O diffusivity of 1 order of magnitude greater reduces α to 0.05, while an order of magnitude

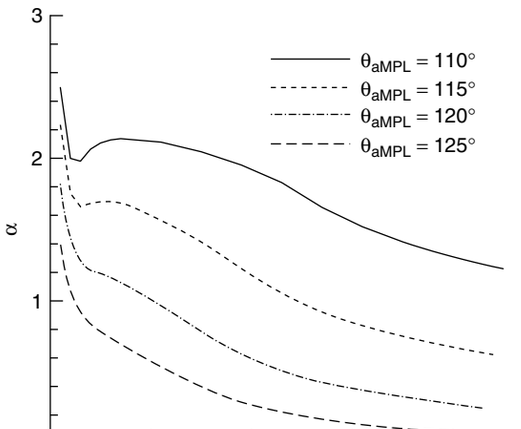

Figure 8. α vs. cell current density for various anode MPL contact angles; anode and cathode stoichiometries of 2.0 @ 150 mA cm^{-2}, and inlet methanol concentration of 2 M; hydrophobic cathode MPL present.

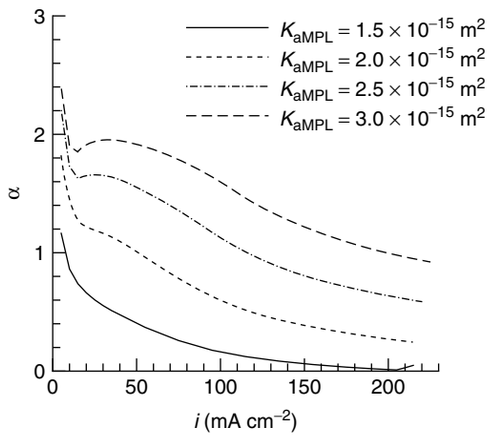

Figure 9. α vs. cell current density for various anode MPL permeabilities; anode and cathode stoichiometries of 2.0 @ 150 mA cm^{-2}, and inlet methanol concentration of 2 M; hydrophobic cathode MPL present.

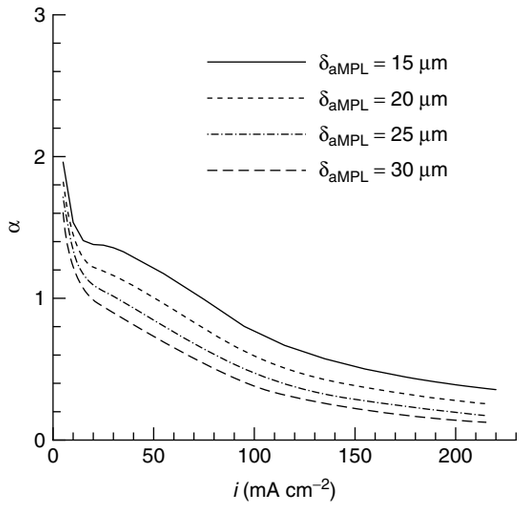

Figure 10. α vs. cell current density for various anode MPL thicknesses; anode and cathode stoichiometries of 2.0 @ 150 mA cm^{-2}, and inlet methanol concentration of 2 M; hydrophobic cathode MPL present.

Table 4. α versus membrane thickness at 200 mA cm^{-2} with anode and cathode MPLs. Note all parameters given in Table 2; anode and cathode stoichiometries of 1.75 @ 150 mA cm^{-2} with 3 M fuel.

δ_{mem} (μm)	α
50	0.293
100	0.527
150	0.654
175	0.695

Table 5. α versus membrane H_2O diffusivity at 200 mA cm^{-2} with anode and cathode MPLs. Note all parameters given in Table 2; anode and cathode stoichiometries of 1.75 @ 150 mA cm^{-2} with 3 M fuel, and $D_o^{H_2O}$ as given in Ref. [29].[a]

$D_{mem}^{H_2O}$	α
$D_o^{H_2O} \times 10^{-1}$	0.878
$D_o^{H_2O}$	0.293
$D_o^{H_2O} \times 10^{1}$	0.050

[a] Reproduced from Ref. [29]. © Elsevier, 2008

lower increases α to 0.878 (our baseline water diffusivity in the membrane is based on the Springer correlation,[31] as described in Ref. [29]). Note that a lower water crossover to the cathode with a thinner membrane is in good qualitative agreement with the experimental findings for low- α MEAs (see Table 1). Aside from low methanol permeability, low methanol EOD, and high proton conductivity, DMFC membranes must also exhibit high water diffusivity. It should be noted that a thin membrane, low- α MEA can be designed to ensure low MCO (∼0.1–0.2) at a given operating current density. However, a thin membrane may yield higher methanol crossover if the current density decreases toward open circuit.

5 SUMMARY AND OUTLOOK

To become more competitive with, and ultimately replace, Li-ion batteries in mobile applications, DMFC systems must be designed to have a higher energy density. To this end, one of the most important goals for DMFC technology is to be able to operate a cell directly on highly concentrated methanol fuel without sacrificing power density. To date, much effort has been expended on reducing methanol crossover, both by means of new membrane development and via various anode fuel delivery designs. However, in this article, we have summarized that, to effectively operate HC-MFCs, the MEA must be designed to not only reduce methanol crossover but also reduce water crossover. Fortunately, developing novel MEA designs that reduce water crossover has emerged as an active area of research and development.

Further, in this article, we have summarized the current state-of-the-art MEA designs by which the water crossover is reduced. Previously, the water crossover reduction was believed to be accomplished primarily by use of hydrophobic cathode MPL.[6, 7, 19–21, 25, 27, 28] Most recently, the addition of a hydrophobic anode MPL has been proven effective in reducing water crossover, and has also been shown to slightly reduce MCO.[23, 24, 26, 29] We have used a 1-D, two-phase transport model to elucidate how water crossover is reduced by incorporation of both hydrophobic anode and cathode MPLs. Additionally, we have used this model to demonstrate how to design the anode MPL to greatly reduce water crossover. In particular, we have shown that a thicker anode MPL with more hydrophobicity and lower permeability is expected to reduce net water transport from anode to cathode. Finally, we showed that a thinner membrane and higher water diffusivity through the membrane, in conjunction with a low- α MEA design, are beneficial in reducing the net water transport into the cathode, possibly even causing net water backflow from the cathode to anode.

As low-α MEA innovation continues and enables the use of higher concentration methanol fuel, there will be an increasing premium on water, as 1 mole of water reacts with 1 mole of methanol in the anode CL. In light of the fact that a 17 M solution has a molar ratio of 1 for methanol to water, this means that, if neat methanol is to be used in a completely passive cell design (i.e., no external water recovery equipment), there must be a back flux of water from the cathode side of the cell to the anode side. It is therefore envisioned that future membrane materials will be developed, which have greater resistance to methanol crossover while simultaneously allowing facile transport of water. Because this dichotomous requirement is difficult to be met by any membrane, there may be a need to design a DMFC with a membrane that facilitates the transport of water, while mitigating the methanol crossover via a combination of novel MPL and CL design and proper operating conditions. Of course, as demonstrated throughout the body of this article, this concept hinges on proper MEA design in order to cause the back flux of water from cathode to anode.

ACKNOWLEDGMENTS

The authors acknowledge numerous contributions of ECEC graduate students, research associates, and industrial collaborators. The writing of this article was made possible, in part, by NSF under grant no. 0609727, National Institute of Standards and Technology (NIST) through ATP program, and ECEC industrial sponsors.

LIST OF SYMBOLS

diff	diffusion
CH_3OH	methanol
CO_2	carbon dioxide
α	net water transport coefficient
β	generic species
c	concentration
D_{mem}	membrane diffusivity
δ	thickness
EW	equivalent weight
ε	porosity
F	Faraday's constant
η_f	fuel efficiency
k_{rl}	liquid-phase relative permeability
i	current density (cell average)
j	diffusion flux
J	Leverett function
K	permeability
λ	water content
i_x	methanol crossover current density
M_l	liquid-phase molecular weight
μ_l	liquid-phase viscosity
n_d	electroosmotic drag coefficient
N_l	liquid flux
N_{mem}	membrane flux
p_c	capillary pressure
p_l	liquid pressure
ρ_l	liquid density
θ	contact angle
s	liquid saturation (i.e., liquid volume fraction of pore space)
σ	surface tension
X_l^β	liquid-phase mole fraction of species β

REFERENCES

1. S. Gottesfeld, 'Polymer Electrolyte and Direct Methanol Fuel Cells', in "Encyclopedia of Electrochemistry, 5", A. J. Bard and M. Stratmann (Eds), John Wiley & Sons, Weinheim, Chapter 8.3, pp. 544–661 (2007).
2. G. Lu and C. Y. Wang, 'Two-Phase Microfluidics, Heat and Mass Transport in Direct Methanol Fuel Cells', in "Transport Phenomena in Fuel Cells", B. Sunden and M. Faghri (Eds), WIT Press, Boston, MA, Chapter 9, pp. 318–358 (2004).
3. C. Y. Wang, *Chem. Rev.*, **104**, 4727 (2004).
4. S. K. Kamarudin, W. R. W. Daud, S. L. Ho and U. A. Hasran, *J. Power Sources*, **163**, 743 (2007).
5. C. K. Dyer, *J. Power Sources*, **106**, 31 (2002).
6. G. Q. Lu, F. Q. Liu and C. Y. Wang, *Electrochem. Solid-State Lett.*, **8**, A1 (2005).
7. F. Liu, G. Lu and C. Y. Wang, *J. Electrochem. Soc.*, **153**, A543 (2006).
8. F. Liu and C. Y. Wang, *J. Electrochem. Soc.*, **154**, B514 (2007).
9. P. S. Kauranen and E. Skou, *J. Electroanal. Chem.*, **408**, 189 (1996).
10. V. Neburchilov, J. Martin, H. Wang and J. Zhang, *J. Power Sources*, **169**, 221 (2007).
11. T. Yamaguchi, F. Miyata and S. Nakao, *J. Membr. Sci.*, **214**, 283 (2003).
12. G. Q. Lu, C. Y. Wang, T. J. Yen and X. Zhang, *Electrochim. Acta*, **49**, 821 (2004).
13. C. Y. Wang, F. Liu, Y. Sato and E. Sakaue, 'Dual-Pump Anode System with Circulating Liquid for Direct Oxidation Fuel Cells', U.S. Patent Pub. No. US 2007/0087234 A1 (2007).
14. M. A. Abdelkareem and N. Nakagawa, *J. Power Sources*, **162**, 114 (2006).
15. W. J. Kim, H. G. Choi, Y. K. Lee, J. D. Nam, S. M. Cho and C. H. Chung, *J. Power Sources*, **157**, 193 (2006).
16. H. F. Zhang and I. M. Hsing, *J. Power Sources*, **167**, 450 (2007).
17. Y. H. Chan, T. S. Zhao, R. Chen and C. Xu, *J. Power Sources*, **176**, 183 (2008).
18. C. Y. Wang, G. Lu, W. Liu, F. Liu, Y. Sato, E. Sakaue and K. Matsuoka, 'Methods to Control Water Flow and Distribution in Direct Methanol Fuel Cells', U.S. Patent Pub. No. US 2006/0134487 A1 (2006).
19. X. Ren, F. W. Kovacs, K. J. Shufon and S. Gottesfeld, 'Passive Water Management Techniques in Direct Methanol Fuel Cells', U.S. Patent Pub. No. US 2004/0209154 A1 (2004).
20. A. Blum, T. Duvdevani, M. Philosoph, N. Rudoy and E. Peled, *J. Power Sources*, **117**, 22 (2003).
21. C. Lim and C. Y. Wang, *J. Power Sources*, **113**, 145 (2003).
22. C. Y. Wang and F. Liu, 'A Paradigm Sift in Direct Methanol Fuel Cell Design for Portable Power', "Proceedings from the 8th Small Fuel Cell Symposium", Washington, DC, Chapter 10, April 2006.
23. F. Q. Liu, 'Optimizing Membrane Electrode Assembly of Direct Methanol Fuel Cells for Portable Power', Ph.D. Dissertation, The Pennsylvania State University, University Park, PA (2006).
24. F. Q. Liu and C. Y. Wang, *Electrochim. Acta*, **53**, 5517 (2008).
25. K. Y. Song, H. K. Lee and H. T. Kim, *Electrochim. Acta*, **53**, 637 (2007).
26. J. Y. Park, J. H. Lee, S. K. Kang, J. H. Sauk and I. Song, *J. Power Sources*, **178**, 181 (2008).
27. U. Pasaogullari and C. Y. Wang, *J. Electrochem. Soc.*, **151**, A399 (2004).
28. C. Xu, T. S. Zhao and Y. L. He, *J. Power Sources*, **171**, 268 (2007).
29. C. E. Shaffer and C. Y. Wang, *Electrochim. Acta*, (2008) submitted.
30. U. Pasaogullari and C. Y. Wang, *Electrochim. Acta*, **49**, 4359 (2004).
31. T. E. Springer, T. A. Zawodzinski and S. Gottesfeld, *J. Electrochem. Soc.*, **138**, 2334 (1991).